International Journal of Thermophysics, Vol. 19, No. 1, 1998

Thermal Diffusivity in Supercritical Fluids Measured by Thermal Lensing

D. E. Wetzler,[1] P. F. Aramendía,[1] M. L. Japas,[2, 3] and R. Fernández-Prini[1, 2]

Received July 15, 1997

Thermal diffusivities of supercritical CO_2 and C_2H_6 were determined over a wide density range with a photothermal technique. The thermal lens, formed by the degradation of the absorbed light energy as heat by the sample, allows the employment of a nonequilibrium method in the critical region. Controlling the refractive-index gradient, i.e., a density gradient, perturbations can be maintained at levels where convection is negligible. An easy-to-operate setup allowed us to measure thermal diffusivities in the density ranges 5 to 20 $mol \cdot dm^{-3}$ for CO_2 at 308 and 313 K and 2 to 12 $mol \cdot dm^{-3}$ for C_2H_6 at 308 K with a standard precision of 15%.

KEY WORDS: carbon dioxide; ethane; photothermal; supercritical fluid; thermal diffusivity; thermal lens.

1. INTRODUCTION

Supercritical fluids have recently attracted attention because of their use as environmentally benign solvents in extraction and separation processes and for carrying out chemical reactions [1]. Therefore, their physicochemical properties have been a subject of intensive study [2]. In the realm of supercritical fluid properties, the determination of transport properties is a difficult task because of the inherent enhanced sensitivity of the medium, due to the divergence of the susceptibilities at the critical point, coupled with

[1] INQUIMAE. Departamento de Química Inorgánica, Analítica y Química Física, Facultad de Ciencias Exactas y Naturales, Universidad de Buenos Aires, Pabellón 2, Ciudad Universitaria, 1428 Buenos Aires, Argentina.

[2] Unidad de Actividad Química, Comisión Nacional de Energía Atómica, Libertador 8250, 1429 Buenos Aires, Argentina.

[3] To whom correspondence should be addressed.

0195-928X/00/0700-0027$18.00/0

the perturbations required to create the gradient which produces the transport. Classical nonequilibrium methods for the determination of thermal diffusivities measure the response of a system to an imposed macroscopic gradient caused by local heating. The response can be measured either under steady-state conditions (by measuring the temperature gradient, related to the thermal conductivity) or by following the time evolution of the temperature of the heated fluid or the propagation of the temperature front in the fluid [3]. As the critical point is approached, temperature gradients have to be limited drastically to avoid the contribution of convection, induced by concomitant density gradients, to the mechanism of thermal relaxation. While classical methods become inadequate in the near-critical region, spectroscopic techniques, such as photon correlation spectroscopy, allow the determination of the diffusivity from the transport mechanisms on a microscopic scale [4]. However, the decreasing capacity of the fluid to scatter incident light forces an increase in the duration of the measurements [5].

The goal of this work was the determination of the thermal diffusivity of a supercritical fluid over a wide density range, including the near-critical region, with the same technique. For this purpose, the study of supercritical carbon dioxide and ethane by a photothermal method was undertaken. These fluids were chosen because of their convenient critical parameters and the availability of thermal diffusivity data over a wide range of densities. The method allows thermal diffusivities to be measured with a 10–20% precision over a very broad density range of the fluid, from the gas-like to the liquid-like domains, with an easy-to-operate and simple setup.

Photothermal methods based on laser excitation are ultrasensitive methods enjoying the advantages of small perturbations and are independent from light scattering since they measure only the heat originated by light absorption [6, 7]. The method presented here, the thermal lens technique, is a classical nonequilibrium method in which a macroscopic thermal gradient is created; it has the advantage that the induced temperature profile is detected through the corresponding change in the refractive index, i.e., the density change, allowing the applied perturbation to be very small (ΔT of the order of 3 to 10 mK). The method also takes advantage of the enhanced susceptibility: the amplitude of the measured signal scales with $(\partial n/\partial T)_p/k$, n representing the refractive index and k the thermal conductivity, diverging at the critical point of a pure fluid. An enhancement of the thermal response of two orders of magnitude was observed by Leach and Harris [8] in supercritical CO_2 at 307 K and 7.84 MPa. A different and more sophisticated photothermal method, laser-induced thermal grating,

was recently employed to measure thermal diffusivities and diffusion coefficients in supercritical CHF_3 [9].

2. THE THERMAL LENS TECHNIQUE

2.1. Description

The thermal lens effect arises when electromagnetic radiation from a focused laser beam is absorbed by an element of volume of a fluid sample. The processes degrading the absorbed energy as heat cause a local increase in the temperature of the medium. If the fluid by itself does not have a suitable absorbance at the laser wavelength, an absorbing probe must be added. In this way a temperature gradient is built up, not only between the irradiated and the nonirradiated regions of the fluid, but also within the irradiated portion itself as a result of the nonuniform spatial distribution of light energy density [6]. In one version of the many photothermal experiments, the sample is irradiated by a focused continuous-wave (cw) laser, normally used in a pure TEM_{00} mode (Gaussian power distribution along the cross section of the beam). The temperature gradient causes a refractive-index change in the fluid, which generates a divergent lens in the irradiated region, thus defocusing the excitation beam. As a consequence of heat diffusion, the heat gradient, which was initially restricted to the irradiated volume, spreads out to the nonirradiated region, changing the focal length of the thermal lens. This change is monitored by measuring the intensity at a small area in the center of the laser beam. The characteristic time for the formation of the thermal lens depends only on the thermal diffusivity of the medium and on the size of the irradiation beam.

The thermal lens technique has been employed basically as an analytical tool to measure the absorbance of low-absorbing transparent liquids [10]. The time evolution of the thermal lens was used to determine thermal diffusion in gases and liquids [11]. There are different versions of the thermal lens experiment; in the single-beam technique employed in this work, the same laser beam is used to induce the refractive-index gradient and to sense the evolution of the formed lens [12].

2.2. Thermal Lens Equations

To describe the time evolution of the formed thermal lens it is assumed that the light power absorbed, P_{abs}, is completely and very rapidly converted into heat compared to the characteristic time of the thermal diffusion process. Thus, heat is delivered to the irradiated volume element at a

rate $P_{th} = P_{abs}$. An absorbing species that fulfills this requirement is called a calorimetric reference [7]. Due to the laser beam spatial distribution of power, a radial temperature gradient is generated. Considering that the illuminated volume has cylindrical symmetry, thermal diffusion will occur only along the radial coordinate r.

The solution of the diffraction equations that describes the effect of the refractive-index gradient on the emerging beam requires some approximations. Two models have been used for this purpose. The "parabolic lens model" [13] approximates the refractive-index distribution as parabolic in the radial coordinate r, to calculate the radius of curvature of the induced lens. The other model, the "aberrant lens model" [14], takes into account the aberrant nature of the formed lens. This is performed by computing the time-dependent focal length of the lens as the superposition of light beams that travel through different optical paths at different radial distance from the light beam center. The temperature gradient is used to calculate the refractive-index variation that changes the optical path. Both models describe the temporal dependence of the beam light intensity at its center, $I(t)$, for a cw laser excitation with TEM_{00}. This intensity, which depends also on Z, the position of the irradiated sample volume relative to the beam focus along the beam direction (see Fig. 1), can be expressed in terms of two parameters: the amplitude θ and the characteristic time t_c.

$$I(t) = I_0 f(Z, t, t_c, \theta) \tag{1}$$

where I_0 is the light intensity at $t = 0$. The parameters in Eq. (1) are related to physical properties of the system, namely,

$$\theta = \frac{P_{th}(-\partial n/\partial T)_p}{\lambda k} \tag{2}$$

and

$$t_c = \frac{\omega^2}{4D} \tag{3}$$

where λ denotes the laser wavelength, ω the Gaussian width of the beam at the sample's position, and D the thermal diffusivity of the sample. The incident laser power P_L and the optical absorbance A are related to P_{th} by

$$P_{th} = P_{abs} = P_L(1 - 10^{-A})$$

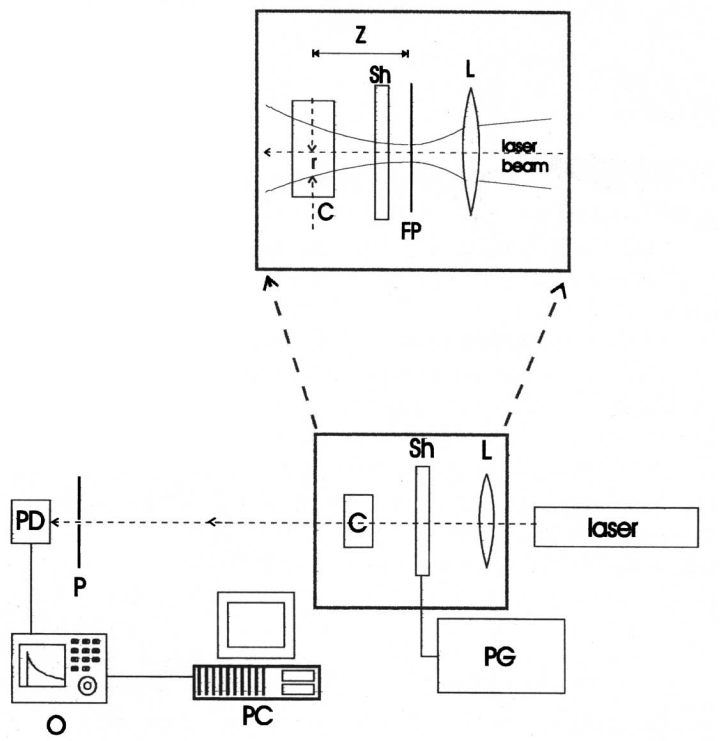

Fig. 1. Schematic representation of the thermal lens setup. The laser is a 632.8-nm He–Ne. L, 150-mm biconvex lens; FP, focal plane of the lens from which the distance Z is measured; C, high-pressure cell; P, pinhole; PD, Si photodiode; Sh, shutter; PG, pulse generator; O, digital oscilloscope; PC, personal computer; r, radial distance across the beam.

which may be approximated to $P_{\text{th}} \cong 2.303 P_{\text{L}} A$ when A is small. The function $f(Z, t, t_{\text{c}}, \theta)$ is model dependent. In the parabolic lens model [13],

$$I(t) = I_0 \left[1 - \theta \left(\frac{2\gamma}{1+\gamma^2} \right) \frac{1}{1 + t_{\text{c}}/2t} \right] \tag{4}$$

while for the aberration lens model [14],

$$I(t) = I_0 \left[1 - \theta \frac{2\gamma}{3 + \gamma^2 + (9+\gamma^2)\, t_{\text{c}}/2t} \right] \tag{5}$$

where

$$\gamma = \frac{Z}{\pi\omega_0^2/\lambda} = \frac{Z}{Z_c} \tag{6}$$

and ω_0 is the Gaussian width of the beam at the focal point. Z_c, as defined by Eq. (6), is called the confocal length.

In both Eq. (4) and Eq. (5) the assumption is made that θ is small, neglecting terms higher than the first power in θ. In Eq. (5) the additional assumption is made that $\tan^{-1}(x) \approx x$ to obtain the factor multiplying θ in the large bracket. It has been shown [15] that, while the time dependence of the lens formation can be represented by either model, the parameters resulting from the fit to the parabolic model do not correspond to the values expected from Eqs. (2) and (3), according to independent measurements of the solvent thermophysical properties. The parameters obtained from the fit to the "aberrant lens," on the other hand, are in agreement with literature data only when the value of θ is small.

Equations (4) and (5) can be expressed in a common form:

$$I(t) = I_0\left[1 - \Theta\frac{1}{1+\tau_c/2t}\right] \tag{7}$$

However, the parameters Θ and τ_c are specific for each model.

For the parabolic lens model,

$$\Theta = \theta(2\gamma)/(1+\gamma^2) \tag{8a}$$

$$\tau_c = t_c \tag{8b}$$

and for the aberration lens model,

$$\Theta = \theta(2\gamma)/(3+\gamma^2) \tag{9a}$$

$$\tau_c = t_c\frac{9+\gamma^2}{3+\gamma^2} \tag{9b}$$

For the above-mentioned reasons, Eqs. (9a) and (9b) were used to interpret the parameters obtained from the fit of the time-dependent thermal lens signal to Eq. (7).

Combining Eqs. (7) and (9b) with Eq. (3), we can obtain values of D from the temporal evolution of the thermal lens formed at a distance Z from the focal plane, provided that the value of ω, or of ω_0, is known (see below).

2.3. Application to the Supercritical Regime

The supercritical domain is characterized by values of the isobaric thermal coefficient $\rho^{-1}(\partial\rho/\partial T)_p$ that increase strongly as the critical point is approached. Consequently, temperature gradients induce increasingly larger density effects, leading to convection. To avoid it, the temperature perturbation has to be reduced drastically, also decreasing the monitoring signal of classical methods. In contrast to this, in the thermal lens technique the evolution of the perturbation is measured by monitoring the refractive index, which is always proportional to the fluid density.

The temperature gradient induced by the absorption of light can be easily estimated for the steady-state conditions: the input power, P_{th}, equals the power flow out of the irradiated volume. From the heat conduction law, the temperature gradient can be calculated from

$$-\frac{\partial T}{\partial r}=\frac{P_{\text{th}}}{k2\pi\omega l}\approx\frac{\Delta T}{r} \tag{10}$$

where $\Delta T=T_{\text{bc}}-T(r)$, T_{bc} and $T(r)$ are the temperatures at the beam center ($r=0$) and at a distance r, respectively, and l denotes the optical length. If we assume that the gradient occurs basically in the illuminated volume, $r\approx\omega$, then

$$\Delta T\approx\frac{P_{\text{th}}}{k2\pi l} \tag{11}$$

Equations (2) and (11) lead to

$$-\frac{\partial n}{\partial T}\Delta T=\frac{\theta\lambda}{2\pi l} \tag{12}$$

where $\lambda/(2\pi l)$ is a constant of the setup. The density effect due to the temperature gradient is

$$\Delta\rho=\frac{\partial\rho}{\partial T}\Delta T=\frac{\partial\rho}{\partial n}\frac{\partial n}{\partial T}\Delta T \tag{13}$$

which, with Eq. (12), gives

$$\Delta\rho=-\frac{\partial\rho}{\partial n}\frac{\theta\lambda}{2\pi l} \tag{14}$$

Equation (14) relates the induced density gradient $\Delta\rho$ to the amplitude of the optical signal θ. Since $\lambda/(2\pi l)$ is constant and $(\partial\rho/\partial n)_p$ is a well-behaved function even in the critical region, Eq. (14) implies that density gradients are always smooth functions of the amplitude θ. Therefore, in the thermal lens technique, convection can be controlled through the value of θ, which depends on P_{th} [cf. Eq. (2)], without loss of sensitivity. In the critical region, where density effects are enhanced, constancy in θ establishes an experimental criterion to maintain a near-constant convection effect. This constitutes the main advantage of the thermal lens method for the study of thermal diffusivities in the critical region.

3. EXPERIMENTAL

The cw setup, similar to the one described in the literature [12, 16], is depicted schematically in Fig. 1. A 2-mW He–Ne laser (Melles Griot) operating at 632.8 nm was employed. The beam was chopped by an electronic shutter (Sh; Melles Griot) and focused in the sample by a biconvex 150-mm-focal length lens (L). The light was detected by a Si diode (PD) positioned at the center of the beam. To sample a small fraction of the beam, the detector had a small aperture (P; a pinhole) and was located far from the sample (about 1.5 m). Neutral density filters were used when necessary to attenuate the laser light intensity. In this way, the value of Θ was always kept below 0.1.

The sample was contained in a 7-mm-optical path high-pressure cell (C) having two sapphire windows. The cell was surrounded by a water-thermostated brass jacket. The temperature was controlled by a Haake unit to within 0.05 K and was measured by a ceramic thermistor calibrated against a standardized Beckmann thermometer (precision, 0.005 K), to within 0.05 K. The ancillary equipment included a high-pressure hand-operated pump and a pressure transducer, calibrated against a deadweight gauge (Ruska; precision, 0.01%). The temperature and pressure calibrations were verified in the sample cell by measuring the vapor pressure of ethane as a function of temperature in the 300–305 K range. Agreement with literature values of the pressure was obtained within 1%. Published equations of state for carbon dioxide [17] and ethane [18] were used to obtain the molar density of the fluids from the experimental pressures and temperatures.

Azulene (Aldrich) was the absorbing dye. To ensure the validity of the thermal lens equations and to avoid solute effects on the measured properties of the supercritical fluids, the azulene concentration was always kept below $10^{-5}M$. Under these conditions, the effect of the dye on the fluid density was kept two orders of magnitude smaller than the uncertainty in

calculating the density with an equation of state through temperature and pressure measurements. Azulene was introduced into the cell by injecting 1 μl of a concentrated toluene solution by means of a microliter syringe. The solvent was allowed to evaporate before sealing the cell. Finally, the cell was repeatedly flushed with the supercritical fluid. Carbon dioxide and ethane were both AGA, 99.99%. Toluene was analytical grade, freshly distilled.

In a typical experiment the sample was irradiated by opening the shutter, which occurred instantaneously in the time scale of the experiment. Due to the formation of the divergent lens, the light intensity at the center of the beam decreased with time, approaching a steady-state value. The diode current was amplified and recorded by a digital oscilloscope. After an adequate time (typically 5 τ_c) the shutter was closed. After an interval longer than the illumination period (typically twice the irradiation period), the experiment was repeated, and the traces were averaged until the signal-to-noise ratio was better than 100. The dark period was adjusted to assure no remaining effect of the previous irradiation.

To determine ω, the laser-intensity distribution across the beam was measured in different ways, depending on the beam size, i.e., on the distance to the beam focus. For large beam diameters, a ca. 0.1-mm pinhole was used; it was displaced perpendicular to the beam propagation direction, by means of a 10-μm-minimum division micrometric screw. The measured diode current as a function of the position was fitted to a Gaussian expression. For beam sizes comparable to the pinhole diameter, a vertical razor blade was placed perpendicular to the beam and was horizontally displaced by the same micrometric screw. In this case, the diode current was fitted to the integral of the Gaussian function.

4. RESULTS

4.1. Determination of ω_0

To calculate D from t_c, the value of ω at the cell position must be known [Eq. (3)]. To measure this quantity and, simultaneously, obtain the fundamental parameter ω_0 for the propagation of the Gaussian beam, the beam intensity profile at different positions was measured. In this way the quality of the laser mode could be tested by fitting the intensity distribution to a Gaussian function

$$I(d) = I_{\max} \exp(-2(d-d_0)^2/\omega^2) \tag{15}$$

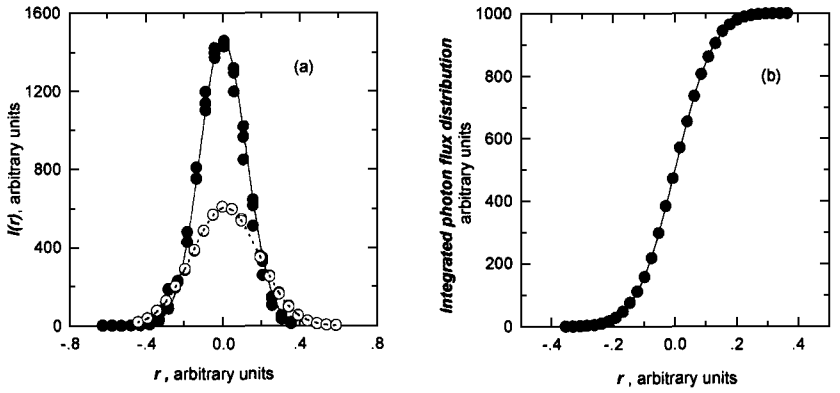

Fig. 2. (a) Photon flux distribution, $I(r)$, across the He–Ne laser beam at two positions, Z, measured from the lens focus. Circles are experimental points and curves are the fit to a Gaussian function [Eq. (10)]. (b) Integrated photon flux distribution at short distances from the focus. The curve is the fit of the experimental points to an integrated Gaussian function.

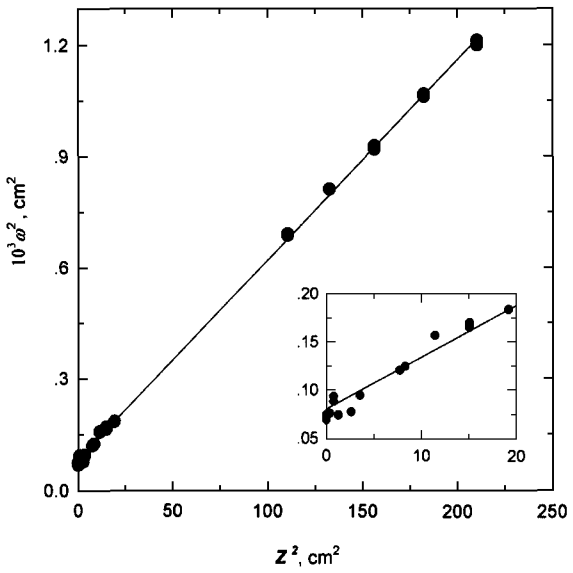

Fig. 3. Plot according to Eq. (11) (see text). ω^2 at each position was obtained from fits similar to those in Fig. 2. The inset shows the detail of points measured near the focal point. From this plot, $\omega_0^2 = (7.48 \pm 0.04)\ 10^{-5}\,\text{cm}^2$ is obtained from the slope.

for positions far from the beam focus, or to its integral, for the small beam widths determined near the focus of the laser. In Eq. (15), r is the radial distance across the beam. Figures 2a and b show the good quality of the TEM_{00} laser used. The value of ω_0 was determined using the Gaussian beam propagation equation:

$$\omega^2 = \omega_0^2\{1 + [Z\lambda/(\pi\omega_0^2)]^2\} = \omega_0^2(1 + \gamma^2) \tag{16}$$

Figure 3 shows a plot of ω^2 vs. Z^2, obtained with the position of the focus calculated from the focal length of the lens as provided by the manufacturer. The value of ω_0 can be obtained from the slope and the intercept of the graph in Fig. 3. The values obtained were $\omega_0^2 = (7.48 \pm 0.04)\ 10^{-5}\ cm^2$ and $\omega_0^2 = (8.04 \pm 0.26)\ 10^{-5}\ cm^2$, respectively. The value of the slope has a lower uncertainty and was therefore used for further calculations.

The validity and consistency of Eqs. (9a) and (9b) were also tested in our setup. For that purpose, the thermal lens signal for azulene in toluene at room temperature and 1 bar was recorded at different positions Z of the

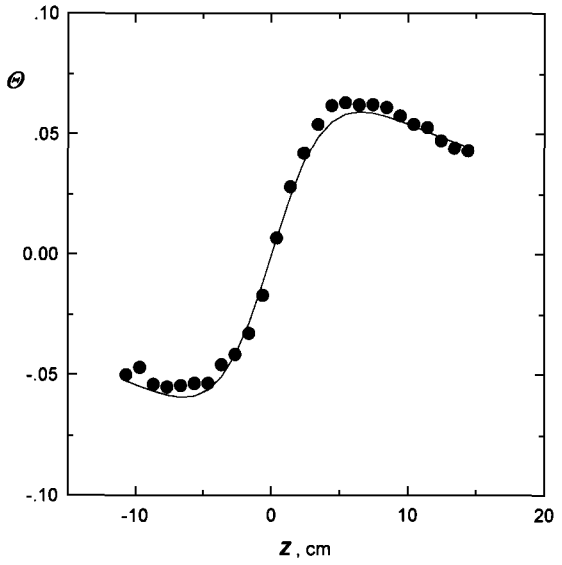

Fig. 4. Thermal lens signal amplitude, Θ, obtained from the fit to Eq. (7), as a function of cell position, Z, measured from the lens focus. Results from azulene in toluene at room temperature and 1 bar. Points are experimental values. The line is the best fit to Eq. (9a).

cell. The time-dependent intensity was fitted to Eq. (7) to obtain Θ and τ_c as a function of Z.

To obtain the full dependence of τ_c on Z, Eqs. (16) and (3) have to be combined with Eq. (9b) to yield

$$\tau_c = \frac{\omega_0^2}{4D} \frac{(1+\gamma^2)(9+\gamma^2)}{(3+\gamma^2)} \tag{17}$$

The values of Θ and τ_c obtained in this way are represented as a function of Z in Figs. 4 and 5, together with their fits to Eqs. (9a) and (17), respectively; the results shown are very satisfactory.

4.2. Thermal Diffusivities of CO_2 and C_2H_6

Thermal diffusivities of carbon dioxide were measured at 308 and 313 K in the fluid density range 3 to 20 mol · dm^{-3}. For ethane, data were taken at 308 K between 2 and 12 mol · dm^{-3}. Temperatures were chosen so

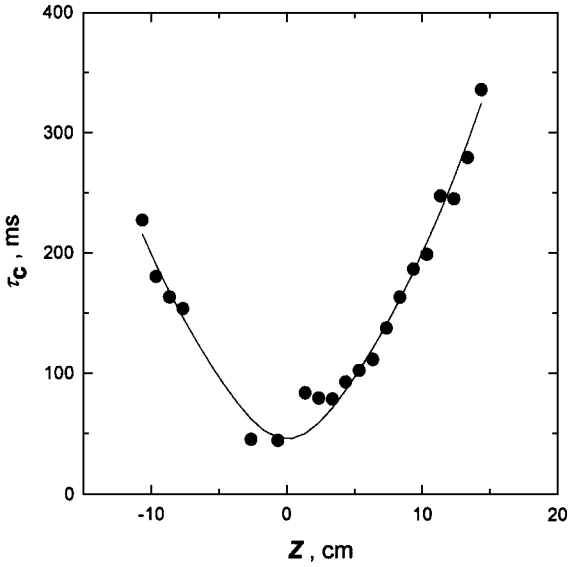

Fig. 5. Plot of τ_c, obtained from the fit to Eq. (7), as a function of cell position, Z, for azulene in toluene at room temperature and 1 bar. Points are experimental values. The line is the best fit to Eq. (12), with ω^2 obtained from Fig. 3.

that literature data exist for comparison [19, 20]. The evolution of the light intensity at the laser beam center was recorded in all cases with the cell positioned at $Z = 3.4$ cm.

Figure 6 shows a signal decay in C_2H_6 and the corresponding residuals to the fit of the data to Eq. (7). The values of Θ and τ_c increase by almost one order of magnitude from the gas-like region to densities near the critical density.

Isotherms of D, as a function of density for CO_2 and C_2H_6, are shown in Figs. 7 and 8, respectively. The values for ethane are on average lower than the literature values by 20% [19]. The deviation increases at high densities. For CO_2 the values of D measured in this work are always higher than the literature values [20]. The deviation is typically 20%, with a dispersion of 15%, with no indication of worsening the results around the critical density. There is no systematic deviation in the temperature or pressure measurements, i.e., in density calculation, that can account for the discrepancy.

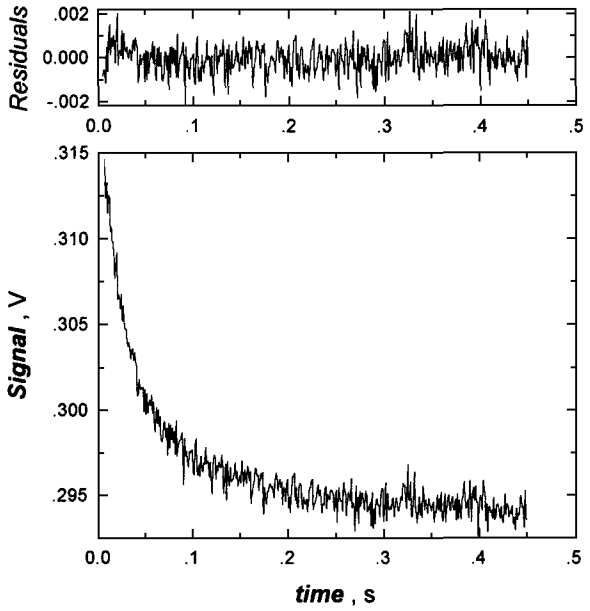

Fig. 6. Time evolution of the light intensity at the laser beam center. The signal was measured in ethane at 307.8 K and density 2.262 mol · dm^{-3} at $Z = 3.4$ cm. In the upper graph the residuals to the fit to Eq. (7) are shown. Fitting parameters are $I_0 = 321.0 \pm 0.5$ mV, $\Theta = 0.091 \pm 0.001$, and $\tau_c = 42 \pm 1$ ms.

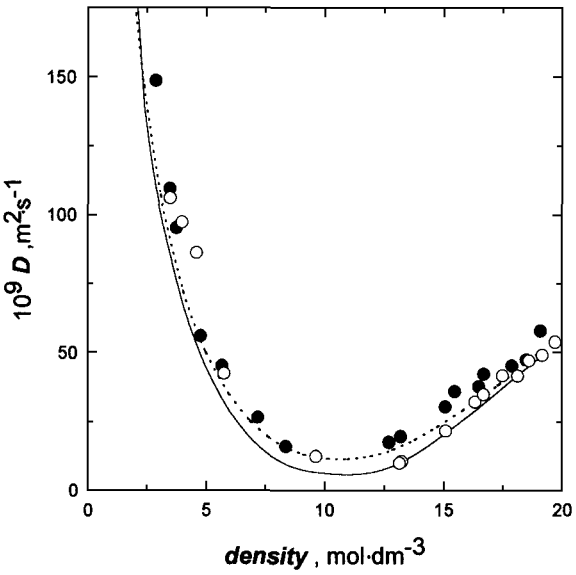

Fig. 7. Thermal diffusivity as a function of molar density for supercritical CO_2 at (○) 308 K and (●) 313 K. Points are experimental results. The curves are smooth fits to literature values [20].

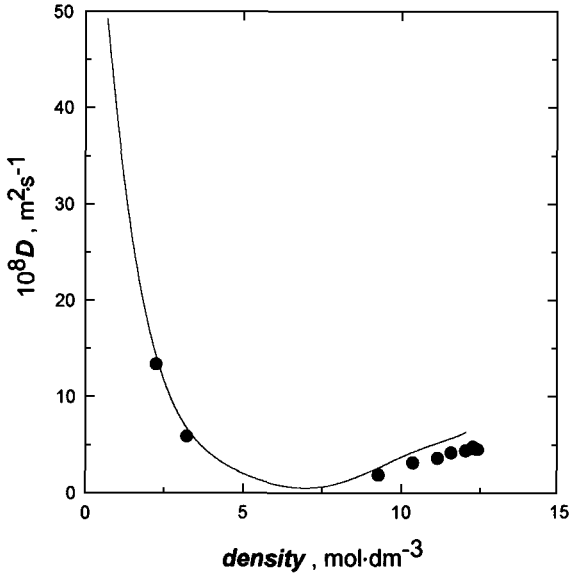

Fig. 8. Thermal diffusivity as a function of density for supercritical ethane at 308 K. Points are experimental data. The curve is a smooth fit to literature values [19].

5. CONCLUSIONS

In spite of the 10–20% accuracy obtained in the present work, the method deserves attention, not only because of its experimental simplicity and affordable setup, but also because of its natural applicability to study both fluid density regimes.

The critical factor in the accuracy attained in the determination of D is the value of ω at the position of the cell. An uncertainty in D of less than 10% will probably be difficult to achieve because of the quadratic dependence of τ_c on the cell position.

Another point worth considering is that, in our setup, a 7-mm cell was used, with a confocal length of 3.7 cm [see Eq. (6)]. The thin lens approximation used in deriving both models might not be valid under these conditions, causing systematic errors. The use of longer focal length lenses should diminish this effect.

REFERENCES

1. P. G. Jessop, T. Ikariya, and R. Noyori, *Nature* **368**:231 (1994). J. M. DeSimone, Z. Guan, and C. S. Elsbernd, *Science* **257**:945 (1992).
2. R. Fernández Prini and M. L. Japas, *Chem. Soc. Rev.* **23**:155 (1994). C. A. Eckert, B. L. Knutson, and P. G. Debenedetti, *Nature* **383**:313 (1996).
3. J. Kestin and W. A. Wakeham, *Physica* **92A**:102 (1978). A. Michels, J. V. Sengers, and P. S. van der Gulik, *Physica* **28**:1201 (1962).
4. N. C. Ford and G. B. Benedeck, *Phys. Rev. Lett.* **15**:649 (1965).
5. A. Leipertz, *Int. J. Thermophys.* **9**:897 (1988). K. Kraft, M. Matos Lopes, and A. Leipertz, *Int. J. Thermophys.* **16**:423 (1995).
6. H. L. Fang and R. L. Swofford, in *Ultrasensitive Laser Spectroscopy*, D. S. Kliger, ed. (Academic Press, New York, 1983), pp. 175-232.
7. G. Heibel and S. E. Braslavsky, *Chem. Rev.* **92**:1381 (1992).
8. R. A Leach and J. M. Harris, *Anal. Chem.* **56**:1481 (1984). R. A Leach and J. M. Harris, *Anal. Chem.* **56**:2801 (1984).
9. D. Kanda, Y. Kimura, M. Terazima, and H. Hirota, *Ber. Bunsenges Phys. Chem.* **100**:656 (1996).
10. N. J. Dovichi and J. M. Harris, *Anal. Chem.* **51**:728 (1979).
11. R. T. Bailey, F. R. Cruickshank, D. Pugh, S. Guthrie, A. McLeod, W. S. Fowlds, W. R. Lee, and S. Venkatesh, *Chem. Phys.* **77**:243 (1983). R. T. Bailey, F. R. Cruickshank, D. Pugh, and W. Johnston, *J. Chem. Soc. Faraday Trans. II* **76**:633 (1980). R. T. Bailey, F. R. Cruickshank, D. Pugh, and W. Johnston, *J. Chem. Soc. Faraday Trans. II* **77**:1387 (1981).
12. J. H. Brannon and D. Magde, *J. Phys. Chem.* **82**:705 (1978).
13. Chenming Hu and J. R. Whinnery, *Appl. Opt.* **12**:72 (1973).
14. S. J. Sheldon, L. V. Knight, and J. M. Thorne, *Appl. Opt.* **21**:1663 (1982).
15. C. A. Carter and J. M. Harris, *Appl. Opt.* **23**:476 (1984).
16. R. M. Negri, A. Zalts, E. A. San Román, P. F. Aramendía, and S. E. Braslavsky, *Photochem. Protobiol.* **53**:317 (1991).

17. J. F. Ely, J. W. Magee, and W. M. Haynes, *Research Report* **110** (Gas Proc. Assoc., 1987).
18. D. G. Friend, H. Inghan, and J. F. Ely, *J. Phys. Chem. Ref. Data* **20**:275 (1991).
19. R. Mosert, H. R. van den Berg, P. S. van der Gulik, and J. V. Sengers, *J. Chem. Phys.* **9**:5454 (1990).
20. A. Michels, J. V. Sengers, and P. S. van der Gulik, *Physica* **28**:1216 (1962).